Title
Quantification of polydimethylsiloxane concentration in turbid samples using raman spectroscopy and the method of partial least squares

Journal
Lasers in Medical Science, 13(1)

ISSN
0268-8921

Authors
Durkin, AJ
Ediger, MN
Pettit, GH

Publication Date
1998-03-01

DOI
10.1007/bf00592958

Lasers Med Sci 1998, 13:32–41

Quantification of Polydimethylsiloxane Concentration in Turbid Samples Using Raman Spectroscopy and the Method of Partial Least Squares

A.J. Durkin[1], M.N. Ediger[1] and G.H. Pettit[2]

[1]Electro-optics branch of the FDA Center for Devices and Radiological Health, Rockville, [2]Autonomous Technologies Corporation, Orlando, USA

Abstract. This paper presents a preliminary application of Raman spectroscopy in conjunction with the chemometric method of partial least squares to predict silicone concentrations in homogenous turbid samples. The chemometric technique is applied to Raman spectra to develop an empirical, linear model relating sample spectra to polydimethylsiloxane (silicone) concentration. This is done using a training set of samples having optical properties and known concentrations representative of those unknown samples to be predicted. Partial least squares, performed via cross-validation, was able to predict silicone concentrations in good agreement with true values. The detection limit obtained for this preliminary investigation is similar to that reported in the magnetic resonance spectroscopy literature. The data acquisition time for this Raman-based method is 200 s which compares favourably with the 17 h acquisition required for magnetic resonance spectroscopy to obtain a similar sensitivity. The combination of Raman spectroscopy and chemometrics shows promise as a tool for quantification of silicone concentrations from turbid samples.

Keywords: Biomedical diagnostics; Breast implant leakage; Optical spectroscopy; Partial least squares; Polydimethylsiloxane (PDMS); Raman spectroscopy; Silicone

BACKGROUND

Silicone-gel implants for breast augmentation and reconstruction have been in use since 1962. In April 1992, the Food and Drug Administration (FDA) restricted the use of silicone gel-filled breast implants, citing lack of adequate information on health risks associated with such implants [1,2]. Local complications have long been known to occur, primarily consisting of capsular contracture, a hardening of the implant to palpation due to contracture of the fibrous capsule that normally forms around the implanted body [3–5]. Ruptures of implants can occur either intracapsularly, or with extracapsular extension and concomitant spread of the gel to the adjacent tissue [6–8]. Although the long-term effects of silicone leakage remain uncertain, published studies to date suggest a rupture rate of 5–51% [2]. The uncertainty in rupture rates is largely due to the lack of a reliable method for detection and quantification of silicone leakage. Virtually all implants have been shown to 'bleed' silicone through their packaging into the local microenvironment [9,10]. This is supported by histological findings of foreign-body granulomas in the capsular tissues or regional lymph nodes [7,11]. More recent observations using magnetic resonance spectroscopy (MRS) have suggested the presence of silicon compounds in the blood of some women with silicone breast implants, as well as evidence of silicon migrating to the liver [12].

A recent report indicates that there may be a small long-term risk associated with silicone implants. However, this study is epidemiological and by no means conclusive [13]. As a scientific adjunct to studies of

Correspondence to: A.J. Durkin, National Research Council Research Associate, FDA/CDRH/HFZ-134, 1901 Chapman Ave., Rm 6, Rockville, MD 20852, USA.

this type, a means for non-invasive determination of the status of implants, and quantification of silicone levels in blood and tissue continues to be a goal of the medical community [14–18].

Detection Methods

Many technologies are currently under investigation for use as potential tools for detection of silicone, but for the most part these suffer from a host of practical difficulties. Although computed tomography (CT) scans produce high resolution images [15], patients are exposed to ionising radiation; therefore CT is not recommended for patients with augmentation mammoplasty [10]. Standard light microscopy histopathological techniques have been shown to be ineffective because silicone is refractile, non-polarisable, non-stainable and therefore difficult to identify [19]. Ultrasonography has been investigated as a method of evaluation of implant integrity but is insensitive to detection of silicone 'bleed-through' [20]. Several laboratories are offering tests that claim to detect levels of antibodies to silicone that presumably indicate a leaking or ruptured implant. However, the very existence of such silicone antibodies has not yet been conclusively demonstrated [10]. There are claims that extremely high antibody levels may indicate a leaking or ruptured implant. However, the clinical significance of silicone antibodies and at what levels these antibodies are harmful remains unknown [16,17]. Although magnetic resonance spectroscopy (MRS) techniques are being investigated to identify implant leaks, they generally suffer from lack of sensitivity in detecting silicone either in small amounts or when silicone is heterogeneously distributed in tissue [12]. In addition, MRS is expensive and time consuming. Finally, standard analytical chemistry techniques such as direct current plasma–atomic emission spectroscopy (DCP–AES) can be used to detect elemental Si in vitro with a sensitivity of 2.0 μg/g (tissue) [18]. These methods, however, cannot differentiate between sources of silicone (PDMS) and elemental silicon, which is often present in non-implant individuals at measurable levels. In addition, these spectroscopic techniques are sample destructive, require extensive sample preparation and are not readily accomplished in a clinical setting.

At present there is no reliable non-invasive technique for determining leakage outside of fibrous capsule. The present work is a step towards determination of the feasibility of such a task using an optical method. Optical spectroscopic methods have become the subject of considerable study as a tool for monitoring the state of tissue. The radiation that is used for these studies, which encompass Raman spectroscopy [21], fluorescence spectroscopy [22], Fourier transform infra-red spectroscopy (FT-IR) [23,24] and reflectance spectroscopy [25] is non-ionising and is amenable to transmission via optical fibre. Spectral data can therefore be acquired using a contact or minimally invasive probe and the efficacy of these various spectroscopies can be studied at a number of organ sites without causing the patient undue risk or discomfort. Although many biologically important molecules can be probed using optical spectroscopy, only limited attempts have been made to interpret tissue Raman spectra in terms of tissue chemical composition [13,26,27]. Raman spectroscopy is particularly attractive because it is a proven tool for sensitive identification of molecular constituents in a mixture of unknowns for non-biomedical applications [28]. Furthermore, recent reports indicate that Raman chemical imaging can be a useful characterisation tool for the identification of polymers, including silicone gel, in the matrix of excised capsular tissue [29–31].

Partial Least Squares

We have used the method of partial least squares (PLS) to develop an empirical linear model of Raman scattering in turbid samples using a training set with known silicone concentrations and optical properties similar to those considered as unknowns [29]. Recently, efforts have been made to quantify chromophores in biological samples using PLS, where work has focused on the determination of blood glucose levels using FT-IR techniques. These preliminary studies have shown promise in the accurate determination of quantitative information from optical spectra both in vitro and in vivo [23,24].

Briefly, using the notation of Malinowski [32] the PLS method is based on the regression between two matrices, **X** and **Y**. For spectroscopic analysis of n mixtures (samples) with p unknowns (constituents of interest), **X** and **Y**

represent spectral and concentration matrices, respectively. Through a sequence of matrix rotations and regression steps, which for the simplest case can be described as a singular value decomposition, PLS seeks to relate the matrix of spectra, **X**, to the matrix of concentrations of the constituent of interest, **Y**, via a calibration or model matrix **B** such that

$$\underset{\mathbf{n}\times\mathbf{p}}{\mathbf{Y}} = \underset{\mathbf{n}\times\mathbf{m}}{\mathbf{X}}\ \underset{\mathbf{m}\times\mathbf{p}}{\mathbf{B}} \quad (1)$$

where **B** is the set of calibration constants for the system. The rows of **X** and **Y** contain information about n sample mixtures. The columns of **X** contain emission spectra at m spectral wavelengths. Although samples may contain many constituents, the rows of **Y** are composed only of the concentrations of the p known constituents of interest for each sample. The reader is referred to a description of non-linear iterative partial least squares (NIPALS) discussed by Malinowski [32] for an accurate and detailed description of PLS mechanics in its least complex manifestation.

The accuracy of prediction for PLS depends on the composition of the training and validation sets as well as the spectral information included in the data [31]. One technique used to assess the accuracy of prediction and to select the optimum number of factors to retain in the model is known as the method of cross-validation [24,32]. This technique evaluates the ability of a PLS calibration model to predict the concentrations of unknown spectra as a function of the rank (number of factors or principal components) used in creating the calibration model. A discussion of cross-validation is included in the Methods section.

An attractive facet of PLS is that it does not explicitly require a priori knowledge of the sample optical properties but does require spectra from a training set of samples with known concentrations and with chemical complexity similar to the unknown sample of interest [24,33,34]. Biological systems are generally complex mixtures for which acquisition of complete chemical information is time consuming and complex, if not impossible. Consequently, the application of PLS methods to Raman spectra presents great potential as a method for optical determination of tissue biochemistry.

METHODS

Samples

To our knowledge, there has not yet been a study that explicitly examines the ability of PLS to predict chromophore concentrations from Raman spectra of turbid media such as blood or human tissue. For PLS to accurately predict concentrations of chromophores in biological samples, it must be shown that the technique can be employed as an accurate predictor in samples that absorb and scatter light. In the case of tissues, scattering coefficients (μs) can range between 50 and 400 cm^{-1} in the ultraviolet and visible portions of the spectrum (250–700 nm), and absorption coefficients (μa) range from less than 1 to greater than 25 cm^{-1} depending on tissue type [35]. In order to examine the predictive ability of PLS using Raman spectroscopy in a tissue-like environment, we performed our study on a series of 40 turbid phantoms with optical properties similar to those of tissue [22,35].

Polydimethylsiloxane (PDMS) was purchased from Sigma Chemical and used without further purification. A preliminary examination of the Raman spectra from pure PDMS gels with viscosity ranging from 20 centistokes (MW=2000), to 500 centistokes (MW=17 250) confirmed that the transitions of interest for the purposes of this investigation can in all cases be found at 490 cm^{-1} and 713 cm^{-1}. It was necessary to include an emulsifying agent in our phantoms so that PDMS would remain diffusely distributed in these mixtures. Sodium dodecyl sulphate (SDS, Sigma Chemical), a common non-ionic surfactant, was first checked for potentially interfering Raman scattering in the wavenumber region of interest and was subsequently mixed with silicone and phosphate-buffered saline (PBS). The introduction of this ingredient to the mix caused microglobularisation of the silicone, resulting in a range of silicone microsphere diameters on the order of 20–100 μm, consistent with silicone particle sizes that have been observed in in vitro investigations performed by other groups [36,37].

Haemoglobin was obtained from blood drawn from the author. Serum was separated from whole blood and discarded according to laboratory standards for the handling of potentially biohazardous fluids. The remaining cells (primarily red cells) were placed in isotonic

PBS (pH 7.4). This was used as a source of oxyhaemoglobin for the remainder of the study. Using previous work with phantoms for quantitative fluorescence spectroscopy as a guideline, samples were mixed so that the final concentration of haemoglobin used in each turbid sample was between 0 and 2% by volume (0–94.6 mM) over the set of 40 samples [22]. A spreadsheet using random number generators and statistical correlation functions was employed in order to ensure that correlation between concentrations of the sample ingredients were minimised. This ensured that the model resulting from the PLS routine would not incorporate artifacts related to simple correlation between sample ingredients or the order in which sample spectra undergo the PLS decomposition. An Eppendorf micropipette (adjustable between 1000 µl and 100 µl) was used to measure the volume of each item placed in the mixtures. After placing PDMS, haemoglobin and surfactant in a non-silicone coated test tube, PBS was added to bring the final volume of each sample up to 10 ml. A complete list of the PDMS and haemoglobin concentrations of each of these samples is described in Table 1. Spectra of the phantoms were acquired using the Raman system described in the next section.

Table 1. Phantom constituents. Turbid phantoms consist of haemoglobin, PDMS, PBS and surfactant. These concentrations are reported in % by volume. The final volume of each sample is 10 ml

Sample number	% PDMS	% HbO
1	6.17	0.07
2	4.03	1.45
3	2.70	0.79
4	9.13	0.76
5	1.00	1.08
6	5.46	0.65
7	4.72	1.27
8	3.45	0.35
9	2.79	0.69
10	1.29	1.79
11	3.60	0.14
12	3.42	1.43
13	0.55	0.80
14	4.69	0.49
15	4.06	0.42
16	9.24	0.93
17	5.88	1.91
18	1.27	0.15
19	0.30	0.69
20	0.22	1.16
21	0.40	0.43
22	4.84	0.55
23	5.47	1.45
24	2.68	0.36
25	7.49	0.30
26	9.15	0.34
27	7.29	1.83
28	9.17	0.25
29	8.70	0.68
30	6.52	1.97
31	6.27	0.67
32	6.97	1.17
33	7.72	1.60
34	3.83	1.38
35	7.03	1.92
36	0.62	0.66
37	2.34	0.40
38	4.18	1.27
39	7.71	1.68
40	0.93	1.94

Experimental Apparatus

The Raman spectrometer used in these studies is depicted in Fig. 1. Light from a 632.8 nm helium neon (HeNe) laser (Spectra-Physics 127) irradiated a plastic cuvette containing approximately 3 ml of sample material. A line pass filter was used to prevent HeNe plasma lines from reaching the sample. The power of the incident light measured at the sample holder was 18 mW. Scattered light was collected from the sample using an optical fibre bundle (manufacturer unknown, 1.9 mm total diameter), placed in close proximity to the illuminated sample spot. Rayleigh scattered light was prevented from reaching the detector using a holographic line filter (Kaiser Super Notch, 6 OD at 632.8 nm). Light entering the spectrograph (SPEX 270 f/4, slit size=50 µm) was dispersed across the face of a CCD detector using a holographic grating (blaze angle=630 nm, 1200 grooves/mm, reciprocal linear dispersion=3.1 nm/mm). The detector was an intensified red/blue enhanced CCD camera (Princeton Instruments ICCD-576G/RBT, 576 × 384 array, pixel size=22 × 22 µm, active area=12.7 × 8.4 mm, peak quantum efficiency=40%). The CCD was thermoelectrically cooled to an operating temperature of −40°C.

The placement of the fibre bundle tip in relation to the sample cuvette was established using a diffuse white reflecting card placed on the inside front surface of a cuvette as a target.

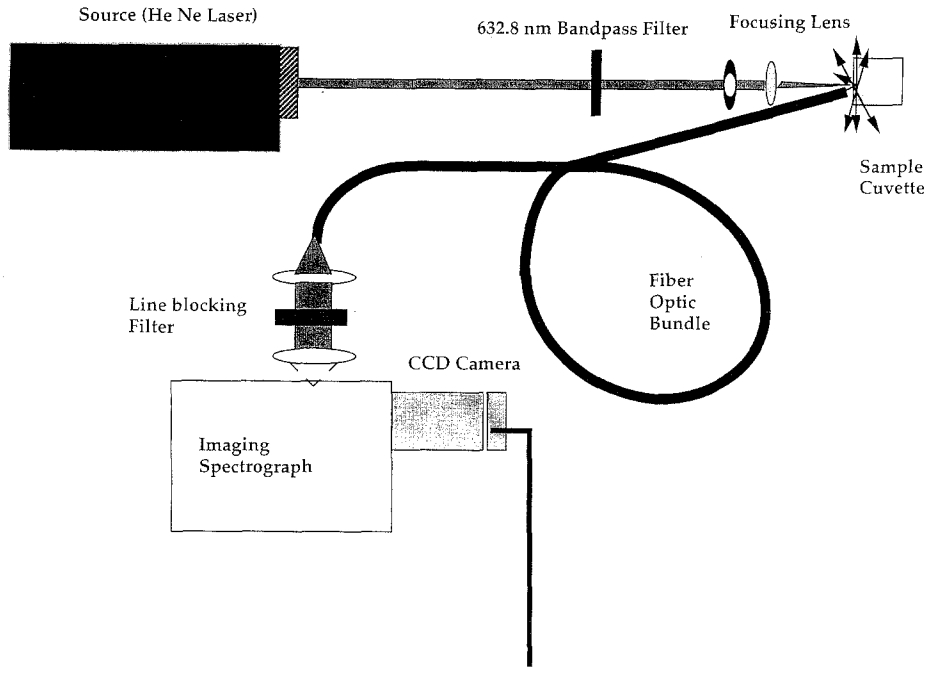

Fig. 1. Experimental set-up. The Raman spectrometer constructed for our preliminary investigations. The source is a 35 mW HeNe laser. Raman spectra were acquired using a cooled, intensified CCD.

This cuvette was filled with water in order to reduce the effect of the index of refraction mismatch between the card and the front of the cuvette. The grating of the spectrograph was adjusted to allow the 632.8 nm line of the laser to fall on the centre of the CCD (pixel number 288). The notch filter was removed and the sample integration time was reduced to 30 ms in order to avoid saturating the detector. The bundle tip was microtranslated until the intensity of the Rayleigh scattered light was maximised.

The optical path, optical fibre collection bundle, cuvettes and test tubes used in this investigation were all tested for silicone contamination and interference in the Raman regime of interest to minimise the possibility of corrupting the experiment. Background interference from the set-up components was tested using a plastic cuvette filled with a mixture of 0.625% 1 μm diameter, monodispersed polystyrene microspheres (Polysciences Inc.) in distilled deionised water. This polystyrene/water mixture was used in order to simulate a sample that might generate sufficient Rayleigh scattered light so as to induce a background Raman signal in the collection arm of the system. Spectra for this scattering sample were acquired over a 5 min period. No potentially interfering signal was observed in the wavenumber region of interest [38].

Calibration and data acquisition were performed using Kestrel Spec software (Rhea Corp.). The 632.8 nm line was used in conjunction with the single point calibration routine provided in the software. Reproducibility of the calibration was verified using the HeNe plasma lines which could be permitted to reach the detector by removing the line pass filter. The integration time for each acquired spectrum was 1 s with a total of 200 accumulated spectra per sample. In order to simulate a device that would not compromise the integrity of whole blood cells, data collection parameters were loosely based on parameters used by various other groups involved in Raman studies of tissues [1,26,39–41]. Real-time compensation for fluctuations in laser power was not possible in this case because a reliable continuous wave detector was not available. However, we were able to account for the slow decrease in laser power over the course of the experiment. To do this, a 'standard' Raman spectrum was acquired, using parameters identical to those used for the turbid samples, from a cuvette containing pure 200 centistokes PDMS every 15 min. This was used to normalise the turbid spectra taken in each 15 min segment. Data were then exported to Microsoft Excel and combined to form matrices. MATLAB (the Math Works, Natick MA) was subsequently used to execute PLS and cross-validation routines.

ANALYSIS

Raw data from the turbid samples in the region of the Raman features of interest (450–750 cm^{-1}) were analysed using a partial least squares algorithm from the MATLAB Chemometrics Toolbox. Background was not subtracted, nor were spectra preprocessed before application of the PLS method. The most accurate prediction model for the training data was chosen using a cross-validation algorithm which would iteratively construct a model for N-1 spectra and treat the remaining spectrum as the 'unknown'. The matrix of the N-1 spectra was then decomposed into principal components, or factors, using singular value decomposition [35]. Models were built using a successively increasing number of these factors. On the first iteration, the model consists of only the factor that accounts for most of the variance in the data (indicated by the magnitude of the corresponding eigenvalue). The model for each factor level was applied to the 'unknown' spectrum to predict the concentration of the component of interest and the prediction error was recorded in a matrix for future reference. The next most important factor (indicated by the magnitude of the corresponding eigenvalue) was subsequently included in the model and the prediction process repeated until a model consisting of all factors resulting from the decomposition of the N-1 training set was employed. The 'unknown' was then returned to the training data and a different spectrum was selected as the 'unknown'. This entire process was repeated until all samples had played the role of 'unknown' once. The prediction error for each factor level was summed across the sample set and plotted. The model for the entire set was then constructed using the factor level for which the residuals across the sample set were minimised. Models consisting of the 'optimum' number of factors+1 and the 'optimum' number of factors − 1 were also constructed. These models were also applied to the data and the predictions compared to the results obtained using the 'optimum' number of factors.

The results of each application of PLS are summarised and discussed in the following section. In each case, an average figure of merit is used to describe predictive ability. The average relative error of prediction (AREP) was calculated via equation 2, as the absolute difference between predicted concentration (P_i) and actual concentration (T_i) averaged over all n samples in the set [22]. This figure was normalised to the maximum actual concentrations of PDMS ($T_{i_{max}}$) making up the phantom.

$$AREP = \frac{1}{n} \sum_{i=1}^{n} \frac{|P_i - T_i|}{|T_i|_{max}} \quad (2)$$

RESULTS

Raman Spectroscopy

Figure 2 illustrates the unique Raman 'fingerprint' of PDMS. The solid line shown here is a typical Raman spectrum of pure PDMS (viscosity=200 centistokes) illustrating the Si-O stretch and Si-C stretch modes that are easily detectable at 490 cm^{-1} and 713 cm^{-1}, respectively. These observed Raman modes are reported to be highly accurate and can serve as specific markers for all silicone products exhibiting unaltered silicon–oxygen and carbon–silicon bands [39]. This region of the Raman spectrum is particularly attractive due to the lack of interfering Raman signal from endogenous tissue constituents [1,26,36]. Contrasted with the spectrum of pure PDMS is a typical spectrum acquired for a sample containing PDMS, red blood cells, SDS and PBS (sample no. 16, Table 1). The change in signal to noise ratio in going from the pure PDMS spectrum to the mixture spectrum helps to illustrate the challenge in recovering accurate concentration predictions of constituents of complex samples.

As discussed above, the appropriate number of factors to use in a predictive model is indicated by the residual predictive errors incurred over the calibration set. Figure 3 indicates the amount of residual error across the sample set as a function of the number of factors used in the model. The residual error for factor levels in excess of eight demonstrates a gradual increase in cross-validation prediction error due to 'overfit' from factors that represent noise. The number of factors for which the minimum in the error occurs is generally a good indicator of the number of factors to keep in the model. It is good practice to verify this by performing concentration prediction using one or two fewer and one or two more factors than that indicated by the minimum. The number of factors suggested by cross-validation for the 40 samples used here is eight. A summary of the AREP of

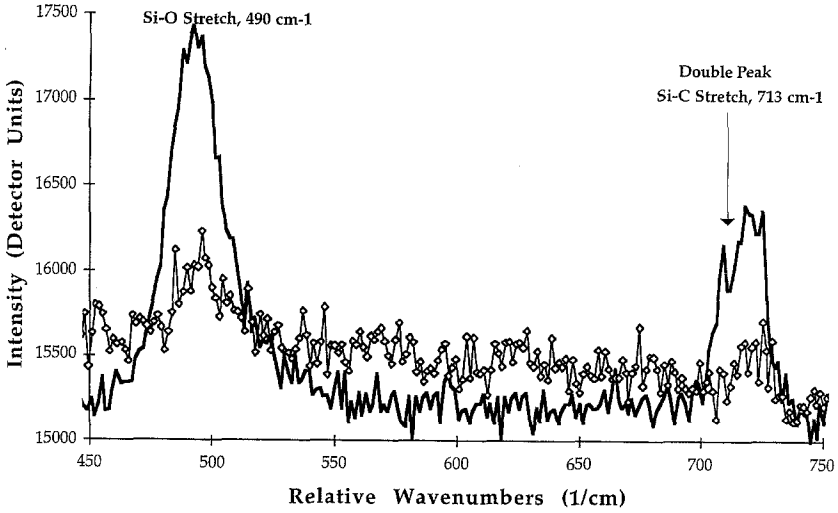

Fig. 2. PDMS spectrum. The solid line is the Raman spectrum of pure PDMS acquired using our setup. The molecular structure is essentially a Si-O-Si- backbone with methyl groups ($-CH_3$) bonded to the Si. The key Raman features shown here are the Si-O stretch (490 cm^{-1}) and the Si-C stretch (713 cm^{-1}). The location of these features is invariant with viscosity (50–500 centistokes). The Raman spectrum for a turbid mixture containing PDMS, red blood cells, SDS and PBS is indicated by the open squares.

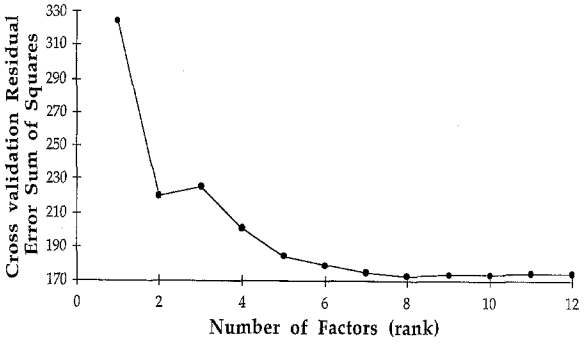

Fig. 3. Residual errors vs number of factors. The appropriate factor level for a model with good predictive ability is generally that level for which the residual errors, summed across the calibration set, are first minimised. In this case, the factor level that minimises the concentration prediction errors is 8.

cross-validation prediction using 4, 6, 7, 8, 9 factors is shown in Table 2 to illustrate how the predictive ability of a model can vary as the number of factors is altered.

Figure 4(a) illustrates the predicted PDMS concentrations obtained by applying PLS to the data acquired for the turbid phantoms. The sum of the residual errors incurred via cross-validation was determined as a function of the number of factors. These results indicated that a model based on eight factors yields the first minimum in residual prediction error across the sample set. This is a reasonable outcome considering that there are three simple constituents (PBS, PDMS and SDS) in addition to blood, which itself is an amalgam of compounds and can contribute a handful of factors to the model itself, depending on the wave

Table 2. Average relative error of prediction (AREP) for cross-validation prediction as a function of the number of factors used in the model

Number of factors	AREP (%)
4	3.82
6	1.12
7	0.79
8	0.55
9	0.58

number region under investigation [41]. The arrow in Fig. 4(a) indicates recent in vitro results obtained using MRS on a blood sample taken from a patient with silicone-filled implants [12]. This corresponds to a PDMS concentration of about 5 mg/g.

In order to approximate a typical application of the PLS technique, a test was performed in which the prediction results obtained by cross-validation were compared to the predictions obtained by application of a model developed for separate training samples. This was done by selecting two sets of 10 samples at random from the original 40 spectra. The predicted silicone concentrations of the first set of 10 samples were calculated using cross-validation. A separate model based on 10 samples not included in this first set of data was also generated using cross-validation. This model obtained for the second set of data was subsequently applied to

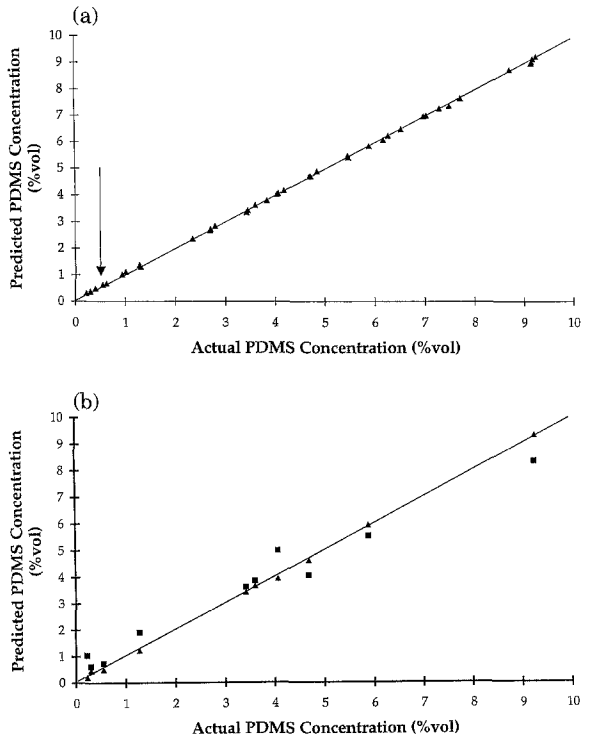

Fig. 4. Prediction of PDMS concentration in turbid samples. The diagonal line has a slope=1. In an 'ideal' investigation, all predictions would lie along this line. (a) Cross-validation prediction results for the entire set of 40 samples. The arrow indicates recent in vitro results obtained using MRS on a blood sample taken from a patient with silicone-filled implants [12]. This corresponds to a PDMS concentration of 5 mg/g of tissue. Our preliminary results based on Raman spectroscopy and PLS compare favourably with this result. (b) Comparison of prediction results obtained by validation (filled squares) to those obtained using cross-validation (triangles).

the first 10 samples. The set one cross-validation predictions are compared to the predictions obtained for set one using the model developed for set two and are illustrated in Fig. 4(b). This result is summarised in Table 3.

CONCLUSIONS

The results of this work indicate that Raman spectroscopy has potential to be useful for the discrete detection of low-concentration foreign compounds in a turbid optical environment. We were able to obtain good agreement between measured and cross-validation predicted silicone concentrations in optically complex samples over a wide range of optical properties. Similarly, we have seen that for a very simple case, application of a model to an independent set of validation data can give predictive results comparable to those achieved via cross-validation. Furthermore, good predictive ability has been demonstrated for PDMS

Table 3. AREP of PLS for cross-validation prediction vs. prediction obtained using a model developed for a separate calibration set

	Validation	Cross-validation
AREP	5.31%	0.59%

concentration regime consistent with a result obtained by a group using magnetic resonance spectroscopy that requires much longer integration time than the Raman method as tested [8]. Work remains to be done to explore the detection limits of this technique.

There is very poor agreement between reported results in the literature. The paper by Garrido et al. [12] which describes MRS as a method for determining blood silicone levels, continues to be the subject of much debate. They reported finding silicone in concentrations of about 5 mg/g. Generally, the rest of the community seems reluctant to accept a concentration of this magnitude, however no one has yet been able scientifically to disprove this result. Furthermore, there is considerable variation between results reported by groups trying to enumerate the differences between background levels of silicon in persons without implants vs those with implants using methods such as DCP-AES, which are sample preparation intensive, but very sensitive (detection limit 2 ng/g) [12,18]. Based on a survey of this literature, we estimate that a sensitivity of 50–100 μg/g will be required. Ultimately, we will have to perform our own experiments (Raman vs DCP-AES) on blood samples from both implanted and non-implanted persons in order fully to understand the detection limits that will be required. We are also currently doing experiments to determine the smallest detectable concentration of silicone in an optically simple sample (PBS, PDMS, surfactant) in order to estimate the limits of detection for PDMS under idealised circumstances.

In the future, we intend to make a number of improvements to gain a greater understanding of the practical limits of this technique. We estimate the collection efficiency for Raman-scattered radiation for these preliminary experiments to be only a few per cent. This leaves considerable room for improvement through modifications to the optical geometry. Towards this end, there have been recent reports of progress in assembling an

optical-fibre based Raman system for biomedical applications. Specifically, a spectroscopy group at Massachusetts Institute of Technology has recently demonstrated a 7-fold increase in collection efficiency of Raman scattered radiation from a tissue surface, using a parabolic reflecting element coupled to an optical fibre [42]. In addition, a group at the University of Texas has had success in obtaining in vivo measurements using an optical probe designed to improve optical throughput and reduce interfering Raman signal from the fibre probe itself [26].

In addition to apparatus modification, application of the PLS method for spectral quantitative analysis is a very active field that is continuously being refined and improved. To date we have applied PLS to the problem of silicone bioassay in a cursory manner. A review of the literature indicates that refinements in both data preprocessing and postprocessing can be used to enhance the predictive ability of the method [43]. These enhancements will be augmented in a synergistic manner by the better Raman spectra (in terms of signal-to-noise ratio) we hope to obtain through the aforementioned modifications.

Finally, we should note that background autofluorescence is a significant concern when performing Raman spectroscopy of human tissue [26]. In the preliminary experiments reported here, fluorescence was not observed to measurably degrade the Raman spectra in the wave number region of interest. As our experiments use progressively more complex samples, eventually using whole blood taken from implant and non-implant patients, this phenomenon will be closely monitored. Methods that have been reported to be effective in combatting these effects include using longer wavelength excitation light and fluorescence subtraction via polynomial fit [1,26,39]. Similar techniques will be invoked as required.

Should these attempts at assay enhancement prove beneficial, a successful diagnostic technique could readily be incorporated into one of the various instruments being developed for optical imaging of the breast. Broader public health benefits include possible low-cost sensitive assays of breast disease, that can be readily integrated into an imaging system. Techniques developed could conceivably be extended to spectroscopic investigations in other organ sites and ultimately may provide a means by which metabolic changes of in vivo tissue can be monitored.

ACKNOWLEDGEMENTS

We would like to thank Stephanie Matchette and Lawrence Grossman from the Electro-optics branch of the FDA Center for Devices and Radiological Health for their helpful consultations regarding sample preparation and PDMS issues. In addition, both the FDA Office of Women's Health and the National Research Council Fellowship programmes provided significant funding for the undertaking of this work and the support of Dr Durkin.

REFERENCES

1. Franck CJ, McCreery RL, Redd DCB, Gansler TS. Detection of silicone in lymph node biopsy specimens by near-infrared Raman spectroscopy. Appl Spectrosc 1993; 47:387–90
2. Kessler DA. The basis of the FDA's decision on breast implants. N Engl J Med 1992; 326:1713–5
3. Gylbert L, Asplund O, Jurell G. Capsular contracture after breast reconstruction with silicone-gel and saline-filled implants: a 6-year follow-up. Plast Reconstr Surg 1990; 85:373–7
4. Brandt B, Breiting V, Christensen L, Nielsen M, Thomsen JL. Five years experience of breast augmentation using silicone gel prostheses with emphasis on capsule shrinkage. Scand J Plast Reconstr Surg 1984; 18:311–6
5. Asplund O. Capsular contracture in silicone gel and saline-filled breast implants after reconstruction. Plast Reconstr Surg 1984; 73:270–5
6. Hausner RJ, Schoen FJ, Mendez-Fernandez MA, Henly WS, Geis RC. Migration of silicone gel to axillary lymph nodes after prosthetic mammoplasty. Arch Pathol Lab Med 1981; 105:371–2
7. Truong LD, Cartwright Jr J, Goodman MD, Woznicki D. Silicone lymphadenopathy associated with augmentation mammoplasty – morphologic features of nine cases. Am J Surg Pathol 1988; 12:484
8. Garrido L, Pfleiderer B, Jenkins BC, Hulka CA, Kopans DB. Migration and chemical modification of silicone in women with breast prostheses. Magn Reson Med 1994; 31:328–30
9. Barker DE, Retsky MI, Schultz S. Bleeding of silicone from bag-gel breast implants, and its clinical relation to fibrous capsule reaction. Plast Reconstr Surg 1978; 61:836–41
10. Teuber SS, Yoshida SH, Gershwin ME. Immunopathologic effects of silicone breast implants. West J Med 1995; 162:418–25
11. Bridges A, Conley C, Burns D, Vasey F. A clinical and immunological evaluation of women with silicone breast implants and symptoms of rheumatic disease. Ann Intern Med 1993; 118:929
12. Pfleiderer B, Ackerman JL, Garrido L. Migration and biodegradation of free silicone from silicone gel-filled implants after long-term implantation. Magn Reson Med 1993; 30:534–43
13. Sanchez-Guerrero J, Colditz GA, Karlson EW, Hunter DJ, Speizer FE, Liang MH. Silicone breast implants and the risk of connective-tissue diseases and symptoms. N Engl J Med 1995; 332:1666–70
14. Centeno JA, Johnson FB. Microscopic identification of silicone in human breast tissues by infrared

microscopy and X-ray microanalysis. Appl Spectrosc 1993; 47:341–5
15. Ahn CY, DeBruhl ND, Gorczyca DP, Basset LW, Shaw WW. Silicone implant rupture diagnosis using computed tomography: a case report and experience with 22 surgically removed implants. Ann Plast Surg 1994; 33:624
16. Rowley MJ, Cook AD, Teuber SS. Antibodies to collagen: comparative epitope mapping in women with silicone breast implants, systemic lupus erythematosus, and rheumatoid arthritis. J Autoimmun 1994; 7:775–89
17. Kossovsky N, Zeidler M, Chun G. Surface dependent antigens identified by high binding avidity of serum antibodies in a sub-population of patients with breast prostheses. J Appl Biomater 1993; 4:281–8
18. Evans GRD, Slezak S, Rieters M, Bercowy GM. Silicon tissue assays in nonaugmented cadaveric patients: is there a baseline level? Plast Reconstr Surg 1994; May 22:1117–20
19. Raso DS, Greene WB, Vesely JJ, Willingham MC. Light microscopy techniques for the demonstration of silicone gel. Arch Pathol Lab Med 1994; 118:984
20. Levine RA, Collins T. Definitive diagnosis of breast implant rupture by ultrasonography. Plast Reconstr Surg 1990; 86:803
21. Manoharan R, Baraga JJ, Feld MS, Rava RP. Quantitative histochemical analysis of human artery using Raman spectroscopy. J Photochem Photobiol B: Biol 1992; 16:211
22. Durkin AJ, Richards-Kortum R. A comparison of methods to determine chromophore concentrations from fluorescence spectra of turbid samples. Lasers Surg Med 1996; 19:75–89
23. Robinson MR, Eaton RP, Haaland DM et al. Noninvasive glucose monitoring in diabetic patients: a preliminary evaluation. Clin Chem 1992; 38:1618–22
24. Haaland DM. Multivariate calibration methods applied to quantitative FT-IR analyses. In: Ferraro JR, Krishnan K (eds) Practical Fourier Infrared Spectroscopy. New York: Academic Press, 1990:395–468
25. Bigio IJ, Mourant JR, Boyer JD. Non-invasive identification of bladder cancer with subsurface backscattered light. In: Alfano RR, Katzir A (eds) Advances in Laser and Light Spectroscopy to Diagnose Cancer and other Diseases. Bellingham, Washington: SPIE Press, 1994:2135
26. Mahadevan-Jansen A, Richards-Kortum R. Raman spectroscopy for the detection of cancers and precancers. J Biomed Optics 1996; 1:31–70
27. Wicksted JP, Erckens RJ, Motamedi M. Monitoring of aqueous humor metabolites using Raman spectroscopy. In: Alfano RR, Katzir A (eds) Advances in Laser and Light Spectroscopy to Diagnose Cancer and other Diseases. Bellingham, Washington: SPIE Press, 1994; 2135:264–74
28. Cooper JB, Flecher PE, Vess TM, Welch WT. Remote fiber optic Raman analysis of xylene isomers in mock petroleum fuels using a low-cost dispersive instrument and partial least-squares regression analysis. Appl Spectrosc 1995; 49:586–92
29. Morris AR, Hoyt CC, Miller P, Treado PJ. Liquid crystal tunable filter Raman chemical imaging. Appl Spectrosc 1997; 50:805–11
30. Schaeberle MD, Karakatsanis CG, Lau CL, Treado PJ. Raman chemical imaging: noninvasive visualization of polymer blend architecture. Anal Chem 1995; 67:4316–21
31. Kidder L, Kalasinsky VF, Luke JL, Levin IW, Lewis EN. Visualization of silicone gel in human breast tissue using new infrared imaging spectroscopy. Nature Med 1997; 3:235–7
32. Malinowski ER. Factor Analysis in Chemistry. New York: John Wiley, 1991:169–72
33. Durkin AJ, Gardner CM, Richards-Kortum R. Comparison of methods for determining fluorophore concentrations from turbid samples, Proceedings from the Conference on Lasers and Electro-optics (CLEO), 1994
34. Thomas EV, Haaland DM. Comparison of multivariate calibration methods for quantitative spectral analysis. Anal Chem 1990; 62:1091–9
35. Durkin AJ, Jaikumar S, Richards-Kortum R. Optically dilute, absorbing and turbid phantoms for fluorescence spectroscopy of homogeneous and inhomogeneous samples. Appl Spectrosc 1993; 47:2114–21
36. Centeno JA, Kalasinsky VF, Johnson FB, Vihn TN, O'Leary TJ. Fourier transform infrared microscopic identification of foreign materials in tissue sections. Lab Invest 1992; 66:123–31
37. Centeno JA, Johnson FB, Kalasinsky VF, Mullick FG, Pestaner JP. Microspectroscopic evaluation of foreign inclusions in human pathology: the laser Raman microprobe technique, Poster presented at United States and Canadian Academy of Pathology, Annual Meeting, Toronto, Canada, 1995
38. Myrick ML, Angel SM. Elimination of background in fiber optic Raman measurements. Appl Spectrosc 1990; 44:565–70
39. Centeno JA, Luke JL, Kalasinsky VF, Mullick FG. Biophysical characterization of silicone breast implants by laser Raman microprobe and infrared microspectroscopy, Preprints of Papers Presented at the 208th ACS National Meeting, 1994; 34:132
40. Berger AJ, Wang Y, Sammeth DM, Itzkan I, Kneipp K, Feld MS. Aqueous dissolved gas measurements using near-infrared Raman spectroscopy. Appl Spectrosc 1995; 49:1164–6
41. Berger AJ, Wang Y, Feld MS. Rapid noninvasive concentration measurements of aqueous biological analytes of near-infrared Raman spectroscopy. Appl Optics 1996; 35:209–12
42. Tanaka K, Pacheco M, Brennan JF et al. Compound parabolic concentrator probe for efficient light collection in spectroscopy of biological tissue. Appl Optics 1996; 35:758–63
43. Small GW, Arnold MA, Marquardt LA. Strategies for coupling digital filtering with partial least squares regression: application to the determination of glucose in plasma by Fourier transform near-infrared spectroscopy. Anal Chem 1993; 65:3279–89

Paper revised 6 May 1997;
accepted after revision 26 September 1997.